Strain-induced change in electronic structure of Cu(100)

D. Sekiba,* Y. Yoshimoto, K. Nakatsuji, Y. Takagi, T. Iimori, S. Doi, and F. Komori[†]

Institute for Solid State Physics, University of Tokyo, Kashiwanoha 5-1-5, Kashiwashi, Chiba 277-8581, Japan

We have studied the electronic structure change of the Cu(100) surface due to the lattice strain both experimentally and theoretically. In the experiments, the surface lattice is compressed by partial nitrogen adsorption. Detailed measurements were made using angle-resolved photoemission spectroscopy with synchrotron and He I radiations. We mainly focused on surface states at the d-band top and bottom, and also sp states (Shockley state) at $\bar{X}$. The d-band bottom shifts toward higher binding energy, while the d-band top shifts toward the Fermi level. This is the direct evidence experimentally indicating the d-band broadening due to the lattice-constant reduction. The observation of the shift of the Shockley state beyond the Fermi level indicates the large electronic redistribution in the sp band. The changes in the electronic structures in the experiments are in good agreement with the results by first-principles calculations. The directions of the energy shifts due to the lattice contraction are well understood by considering the symmetry of the corresponding wave functions at each point of the surface Brillouin zone. An increase of the work function due to the lattice contraction is also discussed in terms of the first-principles calculations. This also implies the special redistribution of Cu $4sp$ electrons, which can significantly influence the chemical reaction on noble metals. Finally, the lattice-constant reduction is quantitatively estimated from the folding point shift of a surface state at the Brillouin-zone boundary.

I. INTRODUCTION

Recently, microscopic lattice strain on metal surfaces has attracted much attention. It has been revealed on the basis of the first-principles calculations that the lattice strain influences various phenomena at the surfaces such as the growth mode of metal thin films[1,2] and catalytic reactions.[3–6] The latter, that is, the chemical reaction changes induced by strain on the surfaces, has been studied experimentally by using scanning tunneling microscopy (STM),[3,7,8] molecular beams,[9,10] and reflection absorption infrared spectroscopy.[11] While these changes originate from that of the electronic structure at the surface, little effort has been devoted to confirming it experimentally so far.[12] To study the electronic structure change of the metal substrate due to the lattice strain, we have chosen the Cu(100) surface as a sample for three reasons. (1) The electronic structure of the clean Cu(100) surface has been well studied both experimentally and theoretically. (2) A well-ordered pattern on the Cu(100) surface partially covered with atomic nitrogen induces a large lattice strain on the clean region.[13–15] (3) Changes in the chemical reaction by the lattice strain were actually observed on Cu(100) previously. Uesugi-Saitow and Yata[9] applied uniaxial tensile stress mechanically on a Cu(100) single crystal and measured the sticking probability of oxygen by means of molecular-beam technique. They observed a slight increase of the sticking probability at a low translational energy of O_2 by increasing the tensile stress. However, it has not been clear whether this stress-dependent change of the sticking probability can be attributed to the lattice strain. The macroscopic increase of the lattice constant under the tensile stress was indeed not observed by diffraction technique. On the other hand, Ohno *et al.*[8] studied the oxygen adsorption on the strained Cu(100) surface induced by the partial N adsorption using STM. They concluded that the reduction of the lateral lattice constant of Cu(100) inhibits the dissociative adsorption of oxygen. This implies that there should be a considerable change of the electronic structure on the Cu(100) surface strained by the partial N adsorption.

In the theoretical studies,[3–6] the relation between the change of the chemical reaction and the lattice strain has often been described as follows. The reduction of the lattice constant will increase the overlap between the wave functions of the adjacent atoms and lead to the increase of the bandwidth. This increase of the bandwidth induces the shift of the d-band center toward the higher binding energy. As a result, the energy gain by the surface reaction to the adsorbates decreases and the surface becomes less reactive. This simple model was developed to explain mainly the experimental data on the Ru(0001) surface,[7] and is called the d-band model. This model gives us an intuitive interpretation of the strain-induced change of the surface chemical reaction in the case of the transition metals, where the localized and partially filled d orbitals dominate the reaction. On the other hand, Sakong and Groß recently made a theoretical study about the dissociative adsorption of H_2 on the Cu surfaces.[6] They showed that the trend of H_2 dissociation probability against the lattice strain depends strongly both on the orientation of the Cu surface and on the contamination on the surfaces.

In the case of Cu surface, the d band is completely filled and the sp band around the Fermi energy can be more important for the chemical reaction. Nevertheless, the role of the sp band has not been paid good attention in the previous theoretical studies on the Cu surfaces.[5,6] The complex but abundant results by Sakong and Groß imply that one has to make clear the strain-induced behavior of each band including the sp band to understand the chemical reaction change due to the lattice strain. The previous theoretical studies on the total density of state (DOS) change integrated over the

surface Brillouin zone (SBZ) will not be sufficient to discuss the relation between the electronic states and the chemical reactions.

In the present study, we show the experimental evidence of the *d*-band broadening and *sp*-band shift of the clean Cu(100) surface due to the lattice compression by angle-resolved ultraviolet photoelectron spectroscopy (ARUPS). In the previous letter,[12] we studied the *d*-band top and reported the energy shift toward the Fermi level. By extending our study to the *d*-band bottom and Cu 4*sp* at $\bar{X}$, we can now discuss the width change of the *d* band and the shift of the *sp* band. These experimental data by ARUPS are carefully compared with the results of first-principles calculations. We discuss the shift direction of individual *sp* and *d* states at high symmetrical points in the SBZ in terms of the symmetry of wave functions.

The paper is organized as follows. The fundamentals of the electronic structure of Cu(100) are introduced in the next section, where the names and locations of states we discuss in the present paper are shown. The structure of the N-adsorbed Cu(100) surface, a part of which is strained clean Cu region, is briefly described in Sec. III. Then the experimental setup for the surface preparations and the ARUPS measurements, and the detail of the first-principles calculations are described in Sec. IV. Section V reports the results of ARUPS at $\bar{\Gamma}$ (Sec. V A), at $\bar{M}$ (Sec. V B), and at $\bar{X}$ (Sec. V C). Sections VI A–VI C show the DOS changes at $\bar{\Gamma}$, $\bar{M}$, and $\bar{X}$ due to the lattice strain, respectively, on the basis of the first-principles calculations. Discussion is made by comparing the results of both ARUPS and the calculation at each point. The symmetry of each wave function is displayed in Sec. VI D. The work-function change due to the lattice contraction is calculated in Sec. VI E. Using the change of the work function evaluated both theoretically and experimentally, we discuss the magnitude of the lattice-constant reduction estimated from the experimental folding point shift in Sec. VI F.

II. ELECTRONIC STRUCTURE OF Cu(100)

First, we briefly introduce the electronic structure of the Cu(100) surface. Figure 1 shows the band map on Cu(100) experimentally determined by Baldacchini *et al.* using the He I radiation as a light source.[16] The surface structure and the corresponding Brillouin zone are illustrated in Fig. 2(d). They surveyed the $\bar{\Gamma}$-$\bar{X}$ and $\bar{\Gamma}$-$\bar{M}$ lines and made detailed comparison with the results of first-principles calculations. They gave names S1–S7 to the surface states and B1–B6 to the bulk states on the $\bar{M}$-$\bar{\Gamma}$-$\bar{X}$ line. We adopted these conventions in the present paper. The M1 state around $\bar{M}$ point at ~-5 eV was named by us because no notation was given in Ref. 16.

Hereafter, we will focus our main attention on S7 at $\bar{\Gamma}$, S4 at $\bar{M}$, and S1 at $\bar{X}$. S4 and S1 are often called the Tamm and Shockley states, respectively. The S7 and S4 states correspond to the bottom and top of the *d* band, so that we can discuss the change of width and center of the *d* band from
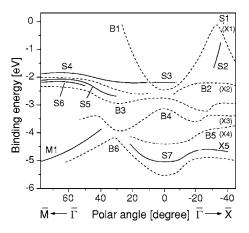

FIG. 1. Schematics of the experimentally determined electronic structure of Cu(100) reported by Baldacchini *et al.* in Ref. 16. The solid lines indicate the bands classified as surface state, while the dotted lines are bulk bands. The notation S and B indicate the surface and bulk bands, respectively. The lateral axis indicates the photoelectron detection angle from the surface normal for He I radiation.

their shifts. While the bottom of M1 at $\bar{M}$ and S7 at $\bar{\Gamma}$ have nearly the same binding energy in experiments, the S7 state might have a slightly higher binding energy. This situation is enhanced in the results of first-principles calculations (see Fig. 8). The S1 state consists of 4*sp* band and is located just below the Fermi level at $\bar{X}$. This state is important to under-
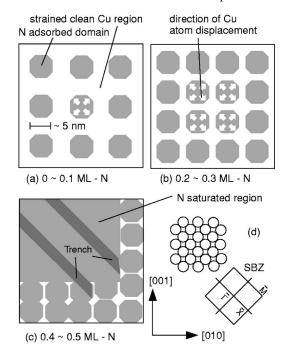

FIG. 2. Schematics of the N-adsorbed Cu(100) surfaces with the N coverage of (a) 0–0.1 ML, (b) 0.2–0.3 ML, and (c) 0.4–0.5 ML. The gray area indicates the N-adsorbed domains, while white area is the clean Cu region. The white arrow in the N-adsorbed domain denotes the expansion of the lateral lattice due to the N adsorption. The dark gray lines in (c) represent the trench which appears on the N-saturated surface. The atomic structure of Cu(100) and the surface Brillouin zone are illustrated in (d).

stand the changes in the chemical reaction and the work function due to the lattice compression because the *d* band is filled with electrons in the present case.

Other surface states such as S5 and S6 at $\bar{\mathrm{M}}$ are discussed later with S4 both experimentally and theoretically. As for M1, we could not separate it from the states due to N 2*p* on the N-adsorbed surfaces in our experimental accuracy. The S3 states have a weak intensity at the edge of the strong projection from the bulk states, and S3 appears as a shoulderlike feature at $\bar{\Gamma}$. The behavior of S3 is reported in Sec. V A together with S7.

The situation around $\bar{\mathrm{X}}$ may require some detailed explanation. One can see X5 at ~-4.5 eV around $\bar{\mathrm{X}}$, which is continuously connected to S7 around $\bar{\Gamma}$. While Baldacchini *et al.* treated this X5 as a part of S7, we regard these as two different states, because they are attributed to different wave functions (see Sec. VI D). Apart from this, the notations X1–X4 indicate the coexistence of surface resonances with bulk states B1, B2, B4, and B5 (see Sec. V C). These resonances were not claimed by Baldacchini *et al.* As for the S2 state, we could not find it mainly because of the overlap of the satellite peaks by the He Iβ radiation and also because of its weak intensity.

III. N-ADSORBED Cu(100) SURFACE

A nitrogen atom adsorbs at the fourfold hollow site of the Cu(100) surface and a $c(2\times2)$ structure is locally formed there. The N adsorption induces a local compressive stress at the surface Cu lattice and leads to a lattice deformation in the surface layers [see the white arrows in Fig. 2(a)].[14] The increase of strain energy limits the area of the N-adsorbed $c(2\times2)$ domain within 5 nm×5 nm. When the N coverage on average is low [0–0.2 ML (monolayer)], the N-adsorbed domains are randomly distributed on a terrace [Fig. 2(a)]. Here, ML is defined as the density of Cu atoms at the 1 ×1 surface. The remaining region is still a clean Cu surface, and the lattice of this clean Cu region is slightly contracted due to the N-adsorbed domains in which the lattice constant is enlarged.

At 0.3 ML of the N coverage, the N-adsorbed domains are periodically arranged on the surface [see Fig. 2(b)]. The domains are separated by narrow Cu belts with clean surface of 2 nm in width, and hence there forms a clean Cu region as large as ~3 nm×3 nm at each intersection of two Cu belts.[13] We call this surface a grid surface hereafter. This pattern is caused by spontaneous strain relief of the lattice in the vicinity of the surface. While the N coverage increases continuously, the lattice constant of the clean Cu region is continuously reduced. This lattice deformation in the clean Cu region becomes maximum on the grid surface. We note that the typical clean Cu region on the grid surface contains ~100 Cu atoms at the surface, and one can still regard it as a two-dimensional Cu surface. Further N adsorption leaves very small clean Cu regions that they no longer possess the electronic properties of the clean Cu(100) surface.

When the N coverage is saturated at 0.5 ML, the surface is fully covered by the $c(2\times2)$ structure [see Fig. 2(c)]. In this case, the strain of the surface lattice is relieved by making trenches of one atomic layer depth. The trench is elongated along the close-packed directions of the Cu substrate (along [110]). The dimension of the trenches is not exactly uniform, and the typical width and length are 1–2 nm and >10 nm, respectively, depending on the terrace size. The trenches are randomly distributed with typical separation of ~10 nm.

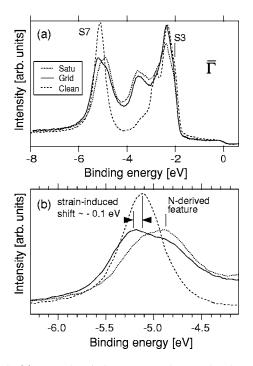### IV. METHODS

A Cu(100) single crystal was cleaned by the cycles of Ar$^+$ ion sputtering and 600 °C annealing. The N adsorption was performed by N$^+$ ion bombardment from nearly surface normal with the beam energy of 500 eV. Then, the sample was annealed at 350 °C for 5 min to make an ordered $c(2\times2)$ arrangement.[13] The coverage of N was changed by the duration of the bombardment. The partially N-adsorbed grid surface (0.3 ML) was confirmed by the $c(2\times2)$ low-energy electron diffraction (LEED) pattern accompanied with the fourfold satellite spots, which indicate the presence of the 7 nm×7 nm ordered superstructure.[17,18] The N-saturated surface (0.5 ML), measured as a reference, can be clearly distinguished from the grid surface by the LEED pattern showing the intense streaks in the [110] direction.

We used the 95 eV *p*-polarized photons at the synchrotron radiation facility KEK-PF, BL18A to study the bottom of the Cu 3*d* band at $\bar{\Gamma}$ by ARUPS. The cross section of the surface state, so-called S7 in the literature,[16] by ARUPS is at a maximum relative to the bulk states at this photon energy.[19] The light incidence angle was fixed at 45° from the surface normal. For the measurements of the Tamm state at $\bar{\mathrm{M}}$ and *sp* state at $\bar{\mathrm{X}}$, on the other hand, He I radiation with a triple mirror polarizer was used as a light source. The photoelectrons were collected in the light incidence plane. The sample temperature was kept below 140 K during all the ARUPS measurements. We used the surfaces with various coverages of nitrogen to discuss the variation of the surface state due to the lattice strain.

We performed first-principles calculations of the electronic states with a symmetric slab model by an extended version of the program package TAPP (Ref. 20) to discuss the experimental results. The same calculation method outlined in the previous letter[12] is adopted. Namely, the slabs and the vacuum region were 19 and 9 atomic layers thick, respectively. Cu atoms were simulated by ultrasoft pseudopotentials. Standard density-functional plane-wave calculations were carried out using the Perdew-Burke-Ernzerhof type exchange-correlation potential.[21,22] The cutoff energy of the plane-wave basis set was 81 Ry. All of the symmetry was utilized, and the number of the irreducible sampled *k* points was $8(8+1)/2=36$. The atomic structures were optimized so that the maximal force acting on an atom became 3×10^{-4} hartree/a.u. A uniform compressive stress was given to the slabs laterally, while interlayer relaxation due to the stress was allowed.

For the calculation of the work function (see Sec. VI E), we used the slabs and vacuum region of 11 and 9 atomic
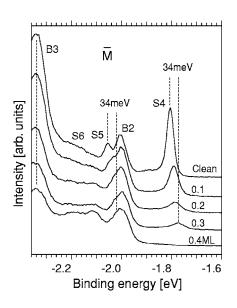
FIG. 3. (a) Normal emission spectra taken on the clean (broken line), grid (solid line), and N-saturated (dotted line) surfaces by 95 eV photon of the synchrotron radiation. (b) Magnification of the spectra around −5 eV from the Fermi level.

layers thick, respectively. The 11 atomic layer thick slabs are sufficient for the discussion on the work function and/or total energy of the system. We prepared thicker slabs to discuss the binding-energy shift due to the lattice strain because we can obtain smoother DOS from the thicker slabs.

V. EXPERIMENTAL RESULTS

A. S7 state at $\bar{\Gamma}$

Figure 3(a) shows the ARUPS spectra at $\bar{\Gamma}$ taken on the clean, grid (0.3 ML N adsorption), and N-saturated surfaces. On the clean surface, we can obtain an intense and sharp peak at ∼−5.1 eV using the synchrotron radiation at 95 eV.[19] By putting nitrogen on the surface, N-derived features develop mainly around ∼−3.5 and ∼−5 eV.

The magnification of the spectra around the S7 state is shown in Fig. 3(b). The peak on the clean surface consists of a single component. On the grid surface, we can see two components at −5.2 and −4.9 eV. While the relative intensity of the peak at −4.9 eV increases with further N adsorption (N-saturated surface), the component at −5.2 eV considerably decreases. Consequently, the feature at −4.9 eV is ascribed to the N 2p state induced by the N adsorption. We can now conclude that the component at −5.2 eV observed on the grid surface is attributed to S7 in the clean Cu region strained by N adsorption. The energy shift of S7 by the lattice strain is estimated to be ∼−0.1 eV toward the higher binding energy.

There is another surface state, S3, indicated by Baldacchini *et al.* at the top edge of the *d* band around $\bar{\Gamma}$. This state

FIG. 4. ARUPS spectra at $\bar{M}$ on the clean and N-adsorbed (0.1–0.4 ML) Cu(100) surfaces. The peaks S4, S5, and S6 are assigned to the surface states, while B2 and B3 are ascribed to the bulk states in the previous report (Ref. 16).

appears at ∼−2 eV also in the spectra in Fig. 3(a) as a shoulderlike feature. We can see the decrease of the S3 intensity with increasing N coverage, while no explicit shift of S3 was observed.

B. S4 state at $\bar{M}$

Figure 4 shows ARUPS spectra at $\bar{M}$. The spectra are normalized with the anode current of the UV source. In this figure, an intense peak of the Tamm state (S4) can be seen at −1.81 eV on the clean surface.[23,24] The intensity of the Tamm state rapidly decreases with increasing N coverage, and it disappears completely on the 0.4 ML surface, where only very narrow clean regions remain. Now we can conclude that there is no Tamm state on the N-adsorbed domain on the grid surface, because both the grid and saturated surfaces have the same local N-adsorbed $c(2 \times 2)$ structure. Therefore, the surface-state peaks at $\bar{M}$, seen in Fig. 4, are the signals only from the remaining clean regions. The strain at the clean region becomes maximum on the grid surface, where the observed Tamm state (S4) shows the binding-energy shift $\Delta E \sim 34$ meV. Another surface state S5 also shows similar modifications of binding energy and intensity. The peaks of B2 and B3 reduce their intensity, but do not show a significant binding-energy change. As for S6, its intensity is too weak for us to discuss the peak shift.

As for the M1 state at ∼−5 eV around $\bar{M}$ (see Sec. II), we made ARUPS measurements with both He I and synchrotron radiations (not shown here). However, we were not able to deconvolute the signals from the M1 and N 2p states for the following two reasons. (1) The M1 and N 2p states have almost the same binding energy. (2) The M1 state is far from $\bar{\Gamma}$ and has a large dispersion, so that the detection angle resolution of our instruments in the beamline for the ∼95 eV
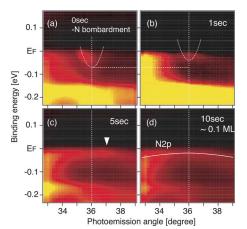
FIG. 5. (Color online) Experimental band dispersions taken on the clean (a), after 1 s (N∼0.01 ML) (b), 5 s (N∼0.02 ML) (c), and after 10 s (N∼0.1 ML) N-bombarded (d) surfaces. The bright area indicates the electronic bands. The vertical dotted line in each panel shows the position of the $\bar{X}$ point determined by the folding point of S1 on the clean surface. The dotted curve in (a) indicates the band dispersion of S1. The dotted curve in (b) is the deduced band dispersion of S1 on the strained surface. The horizontal dotted line connecting (a) and (b) is a guide to the eyes to see the upward shift of S1. The white triangle in (c) indicates the peak ascribed to the bottom of S1. The black curve in (d) shows the dispersion of the N-derived band on the N-adsorbed domain.

photon was not enough to discuss the subtle shift of M1 due to the lattice strain. On the other hand, the cross section of M1 for the He I radiation was too small, though the angle resolution of the apparatus in the laboratory was enough.

The states at the top of the Cu $3d$ band including the Tamm state shift toward the Fermi level. In the previous section, on the other hand, the S7 state at the bottom of the Cu $3d$ band shifts toward the higher binding energy. Thus, the d-band width enlargement due to the lattice compression was experimentally confirmed by ARUPS.

C. S1 and X1 state at $\bar{X}$

Figure 5 shows the experimental band dispersions in the vicinity of the Fermi level around $\bar{X}$ for four different samples with N coverage between 0 and ∼0.1 ML. The bright region indicates the electronic bands. The photoemission spectra were taken between 33° and 39° of detection angle from the surface normal by multichannel plate simultaneously. On the clean surface, we can see a parabolic band dispersion [dotted curve in Fig. 5(a)] very close to the Fermi level. This band consists of the Cu $4sp$ states, and is named S1 in the literature[16] and is conventionally called the Shockley state. This state was experimentally reported by Kevan.[25,26] He used the Ne I radiation (16.85 eV) and estimated the maximum binding energy of this state as −58±5 meV. Recently Schiller *et al.* claimed that this S1 state is above the Fermi level and occupied by thermally activated electrons at room temperature (RT).[27] As can be seen clearly in Fig. 5(a), the bottom of the S1 state is below the Fermi level at 140 K in our results. We estimated the
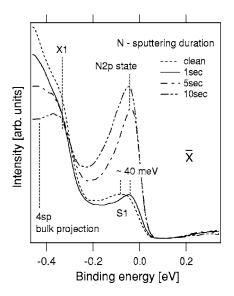

FIG. 6. ARUPS spectra at $\bar{X}$ near the Fermi level after N bombardment of 0, 1, 5, and 10 s. The angle resolution for the photoelectron detection is set at 0.2°.

binding energy of the bottom as ∼−60 meV. Possible reasons to explain the results of Schiller *et al.* are a slight tilt of the sample surface from the exact X point and/or the thermal expansion of the lattice at RT.

After 1 s N bombardment, where the N coverage is ∼0.01 ML, there appeared very weak $c(2 \times 2)$ spots in the LEED observation. On this surface, a small number of N-adsorbed domains were formed in the wide clean terraces with a slight lattice strain. We can see the spot of the S1 state [indicated by dotted curve in Fig. 5(b)] in the experimental band dispersion on this surface, while the background due to a N-derived state develops at the same energy region. The bottom of the S1 state now shifted up to ∼20 meV below the Fermi level. On the surface with 5 s N bombardment (N ∼0.05 ML), we can see clearly the N-derived state with a little dispersion, which is close to the Fermi level at $\bar{X}$ and turns toward the higher binding energy. There still exists a faint signal near 37° [indicated by a white triangle in Fig. 5(c)] on the N-derived features. This might indicate the bottom of the S1 state. After 10 s N bombardment (N∼0.1 ML), there is no signal from the S1 state around the Fermi level and only the N-derived feature is recognized [see the solid curve in Fig. 5(d)]. We note that even on the surface with 0.1 ML N coverage, 80% of the surface is still clean. Consequently, we conclude that the shift of the S1 state is mainly attributed to the reduction of the lateral lattice constant, while the contamination effect from the N-adsorbed domain is somehow convoluted because the Cu $4sp$ state is highly delocalized.

The change of the electronic structure at $\bar{X}$ by lattice strain and N adsorption can be seen quantitatively in spectra around $\bar{X}$. Figure 6 shows the ARUPS spectra taken on Cu(100) with the same N-bombardment duration discussed in Fig. 5: clean, 1, 5, and 10 s. On the clean surface, there are the peak of S1 around −60 to−80 meV and also the precipice from −0.3 eV, which mainly consists of the bulk $4sp$
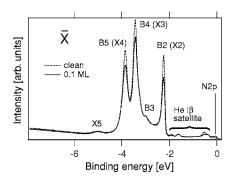
FIG. 7. ARUPS spectra at $\bar{X}$ of the clean and 0.1 ML N-adsorbed surfaces for the binding energy between −8 and 0 eV. The broken and solid lines indicate the spectra on the clean and 0.1 ML N-adsorbed surfaces.

projection. After 1 s N bombardment, we can see the development of states at the Fermi level and the S1 shift ΔE $\sim$40 meV. More N bombardment (5 and 10 s) induces the intense N 2p-derived feature at the Fermi level. Nevertheless, we can conclude from the two-dimensional plot in Fig. 5(b) that the shifted peak observed after 1 s N bombardment is the surface state instead of the N 2p state. On the other hand, the DOS of the 4sp bulk projection is also changed by N adsorption. After 1 s N bombardment, the edge intensity of the precipice at $\sim$−0.3 eV decreases, indicating the existence of a surface resonance. We call this surface resonance X1 henceforth. While further N bombardment does not apparently modify the edge shape, the intensity of the deeper binding-energy region $\sim$−0.45 eV drops rapidly. We will discuss these behaviors with the results of the first-principles calculations in Sec. VI C.

We mention here other surface states at $\bar{X}$. Figure 7 shows the ARUPS spectra at $\bar{X}$ with the binding energy between −8 and 0 eV by the He I radiation. The spectra on the clean and 0.1 ML N-adsorbed surfaces are compared. We can see five distinct peaks notated as B2–B5 and X5 in the d-band region on the clean surface. The above-mentioned S1 and X1, and also S2 claimed by Baldacchini *et al.*, are not visible with this energy resolution. After 0.1 ML N adsorption, we can see the considerable decrease of the intensities of B2, B4, and B5, while the intensity of B3 does not change. This implies the coexistence of surface resonances with B2, B4, and B5. We named these resonances X2, X3, and X4. The shifts of X2, X3, and X4 were not observed in our experimental accuracy. On the other hand, we observed that the intensity of X5 slightly decreases with the 0.1 ML N adsorption, while no explicit peak shift was found. The synchrotron radiation was also not useful for the investigation of X5 for the same reason as for M1 at $\bar{M}$.

VI. DISCUSSION

A. DOS change at $\bar{\Gamma}$

The top panel of Fig. 8 shows the calculated DOS at $\bar{\Gamma}$ constructed by Lorenzians possessing 0.01 eV width. The solid line and dotted line indicate the normal and −2%
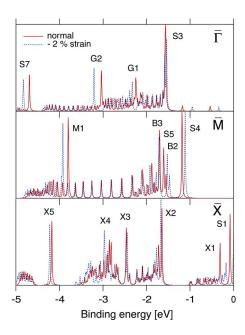

FIG. 8. (Color online) Calculated DOS of the normal (solid line) and −2% strained (dotted line) surfaces at the $\bar{\Gamma}$ (top), $\bar{M}$ (middle), and $\bar{X}$ (bottom) points in SBZ. The calculated DOS consists of 100% of the topmost layer, 50% of the second layer, and 25% of the third layer to simulate the photoemission spectra accounting for the escape depth of the photoelectrons. The normal and −2% strained surfaces are plotted in red and blue in the electronic version.

strained surfaces, respectively (red and blue in the electronic version). Here, the calculated DOS consists of 100% of the topmost layer, 50% of the second layer, and 25% of the third layer to simulate the photoemission spectra accounting for the escape depth of the photoelectrons.

We can see four distinct peaks at $\sim$−1.55 eV (S3), $\sim$−2.24 eV (G1), $\sim$−3.04 eV (G2), and $\sim$−4.68 eV (S7) in the figure. We can assign the peak at $\sim$−4.68 eV in the calculation to the S7 peak in the experimental spectra of the clean surface for the following two reasons. First, both experimental and theoretical peaks are located at the bottom of Cu 3d states. Second, the calculations indicate the even symmetry of this state with respect to the $\bar{\Gamma}$-$\bar{M}$ line, as will be shown later. This agrees with the observation that the peak was detected by p-polarized photon along the $\bar{\Gamma}$-$\bar{M}$ direction. It is also acceptable to assign S3 to the shoulderlike feature in Fig. 3(a), because both are located at the top edge of the d band at $\bar{\Gamma}$. As for the other two peaks, G1 and G2, in the calculations, we might assign them to the experimental peaks at $\sim$−3.0 and $\sim$−3.5 eV, respectively, while the binding energies of G1 and G2 in the calculated DOS including a number of bulk 3d states are quantitatively unreliable.

By reducing the lateral lattice constant (−2%) in the calculation, we can see the apparent shifts of G1, G2, and S7 toward the higher binding energy, while the shift of S3 is negligibly small. At $\bar{\Gamma}$, the d-band width is expanded and the band center shifts toward the higher binding energy by lattice compression. The S7 shift of $\Delta E\sim$−0.1 eV toward higher binding energy in the calculations agrees very well with the experimental result. The quite small shift of S3 in the calcu-
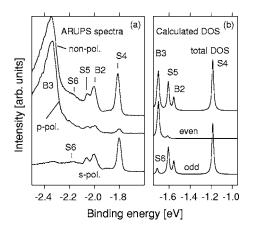
FIG. 9. (a) ARUPS spectra at $\bar{M}$ taken on the clean surface with nonpolarized (top), p-polarized (middle), and s-polarized light (bottom). The names of peaks B2, B3, S4, S5, and S6 are referred from a previous report (Ref. 16). (b) Calculated DOS of unstrained Cu(100) surface. The top spectrum shows the total DOS of the topmost three surface layers (see main text). The even and odd symmetry components of this DOS are also displayed in the middle and at the bottom, respectively.

lations is consistent with the experimental results that the intensity of the shoulderlike feature decreases without any shift in our experimental accuracy. On the other hand, it is difficult to compare the calculations with the experimental results for the shifts of G1 and G2 peaks because of the complex convolution of the surface resonance, bulk, and N-derived states.

B. DOS change at $\bar{M}$

The middle panel of Fig. 8 shows the calculated DOS at $\bar{M}$. We can see five intense peaks at -1.18 eV (S4), -1.56 eV (B2), -1.61 eV (S5), -1.70 eV (B3), and -3.80 eV (M1). First, we discuss the electronic states around the d-band top, namely, S4, B2, S5, and B3. These states between the experiment and calculation were carefully assigned in terms of the electron orbital symmetry and selection rules for the polarized photons. Middle and bottom curves in Fig. 9(a) show the ARUPS spectra at $\bar{M}$ with p and s polarizations, respectively. Here the degree of light polarization is 90%. Relative to the B3 intensity, those of B2, S4, and S5 are strongly suppressed and S6 is now invisible in the data of p polarization. Opposite to the s polarization, B3 feature is reduced, whereas B2, S4, S5, and S6 are clearly seen. From these data, we know that B3 has even symmetry with respect to the $\bar{\Gamma}$-$\bar{M}$ line, while B2, S5, S6, and S4 have odd symmetry. We also resolved the calculated DOS into even and odd components as the middle and bottom curves in Fig. 9(b). In the even component of the calculated DOS, there is a unique distinct peak around ~-1.7 eV, and we should assign this to B3. A small peak next to B3 in this component may not be detectable in the experiment. Four features are observed in the odd component around ~-1.65, ~-1.60, ~-1.58, and ~-1.2 eV, and it is reasonable to attribute them to S6, S5, B2, and S4, respectively.

Now, we return to the middle panel of Fig. 8, where the results of the DOS calculation at $\bar{M}$ without and with the -2% lattice constant reduction are shown by the solid and dotted curves, respectively. The same procedure described in Sec. VI A was adopted to take into account the photoelectron escape depth as in the top panel of Fig. 8. According to these calculated results, the Tamm state S4 ($\Delta E \sim 67$ meV), S5 (~ 80 meV), and B2 (~ 80 meV) move toward the Fermi level, whereas B3 goes slightly to larger binding energy. These trends for the surface states are in good agreement with the experimental results (Fig. 4) except that no energy shift of B2 was observed in the experiment.

The discrepancy for B2, however, is attributed mainly to the simple assumption in the present model and the origin of the photoelectrons as follows. First, the strain is strongly localized at the first few layers on the N-adsorbed Cu(001) surface,[14] while in the calculation, the compressive strain was uniformly given throughout the slab. The B2 state in the calculation has the maximum partial DOS in the layers deeper than the third layer. In such a bulk region, however, the net strain on the sample from the N-adsorbed domain is much smaller than that of the first layer in the present sample. Second, the B2 signal includes photoelectrons coming from the bulk region below both the clean region and the N-adsorbed domain where the lattice constant is increased. Consequently, the B2 signal may consist of two features: one from the clean region moving slightly toward the Fermi level and the other from the N-adsorbed domain moving slightly to higher binding energy. In fact, the B2 peak just broadens with increasing the N coverage, while its center is at the same position.

We also calculated the electronic structure of the system with 2% expanded lattice constant to confirm the above discussion (not shown in the figure). The result shows a linear response, i.e., S4 ($\Delta E \sim -60$ meV), S5 ($\Delta E \sim -50$ meV), and B2 ($\Delta E \sim -72$ meV) move away from the Fermi level, while B3 stays almost at the same position. This confirms that the peak shifts in the calculation are caused by the change of the lattice constant, not by any other artifacts.

On the other hand, we can see that the M1 peak shifts toward the higher binding energy $\Delta E \sim -120$ meV in the middle panel of Fig. 8. Hence at $\bar{M}$, both the d-band width and its center energy increase with decreasing the lattice constant as in the case at $\bar{\Gamma}$. In the experiment, however, we could not clearly confirm the M1 shift even by using the synchrotron radiation because the intense peak due to N $2p$ covers it in the same binding-energy region.

C. DOS change at $\bar{X}$

The DOS change in the calculations at $\bar{X}$ is shown in the bottom panel of Fig. 8. Four major peaks X2–X5 are observed in the d-band region, and the Cu $4sp$ state (S1) is found near the Fermi level. We can find also a surface resonance named X1 just below S1 at the edge of the $4sp$ bulk projection.

The response of the d band at $\bar{X}$ for the lattice strain is relatively small. The slight shift of X5 toward the higher

binding energy results in the enlargement of the *d*-band width at $\bar{\mathrm{X}}$. On the other hand, large shifts are indicated for the S1 and X1 states with the lattice strain, and S1 moves above the Fermi level. This explains well the experimental results for S1 shown in Figs. 5 and 6.

We could not observe the distinct peak of X1 in the ARUPS spectra in Fig. 6, while the edge intensity of the 4*sp* bulk projection at ∼−0.3 eV can be ascribed to the X1 state. As shown in Fig. 6, the intensity at the edge of the 4*sp* bulk projection decreased after 1 s N bombardment. The same behavior was also observed in the vicinity of $\bar{\mathrm{X}}$. These are consistent with the theoretical results that X1 shifts toward the Fermi level with decreasing intensity because of the lattice strain. The complex change in the bulk *sp*-band region just below X1 in the calculated DOS may correspond to the large change of the spectral feature around −0.4 eV with higher N coverage in Fig. 6.

The existence of the three intense peaks X2–X4 agrees with the dramatic decrease of intensities of B2, B4, and B5 by N adsorption in Fig. 7. In the experiments, X2–X4 are included as surface resonances in the spectral features of B2, B4, and B5. The small shifts of X2 and X3 in the calculations are consistent with the experimental results that there were no significant shifts in the B2 (X2) and B4 (X3) peaks. While X4 considerably shifts toward the higher binding energy in the calculations, we found no shift of B5 (X4) peak by ARUPS in our experimental accuracy. This may be explained by the strong convolution with the numerous bulk states around X4.

As for the X5 state at ∼−4.2 eV, the cross section of X5 for the He I radiation was too small to confirm the shift of X5 in the calculations. Furthermore, according to the calculated DOS in the bottom panel of Fig. 8, the shift of X5 is little compared with that of S7 and M1. This may be the reason why we could not detect the shift of X5, which has a broad and weak spectral feature.

D. Level shifts and the symmetry of wave functions

The shift direction of each electronic state can be qualitatively understood by considering the symmetry of the wave functions in real space, that is, the tight-binding or linear combination of atomic orbital representation is useful. The upper panel of Fig. 10 shows the calculated wave functions of S3, G1, G2, and S7 at $\bar{\Gamma}$, which appear in the top panel of Fig. 8. The rectangular parallelepiped indicates the unit cell of the Cu slab. The Cu atom in the topmost layer is located at the center of the square at the top of the parallelepiped, and the Cu atom in the second layer is at each corner of the square as shown by broken lines in the figure of the G1 state. The S3 peak consists mainly of three components: d_{xy} at −1.56 eV and d_{xz} and d_{yz} at −1.58 eV notated as S3-(1), S3-(2), and S3-(3), respectively. The d_{xz} and d_{yz} have considerable bulk components. The G1 peak has $d_{3z^2-r^2}$ component of the topmost layer. The G2 peak is constructed by $d_{x^2-y^2}$ components of the three layers at the surface. The S7 peak, the shift of which we confirmed experimentally, is mainly ascribed to the $d_{3z^2-r^2}$ states of the first and second layers.

In the calculated DOS at $\bar{\Gamma}$ (Fig. 8, top), G1, G2, and S7 shift toward the higher binding energy by the compression of the lattice, while S3 showed quite a small shift. The chemical bonds of these states with the nearest neighbors are schematically shown in Fig. 11 in terms of the tight-binding representation. The light and dark gray colors in Fig. 11 indicate the symmetry of the wave function. We can clearly see that G1, G2, and S7 construct bonding-type Bloch functions at $\bar{\Gamma}$. The reduction of the lattice constant enhances the overlap of adjacent wave functions, so that the bonding-type chemical bonds become more stable. This will lead to the shift of G1, G2, and S7 states toward the higher binding energies.

The wave functions of S3-(3) make bonding-type π bonds along $[1\bar{1}0]$, while they make antibonding-type σ bonds along $[110]$. The similar arrangement of wave functions is constructed also for S3-(2). On the other hand, S3-(1) constructs the antibonding-type Bloch function along both directions. In general, the σ bond dominates the π bond, and thus, the total S3 would shift toward the Fermi level with the decrease of the lattice constant. The discrepancy that S3 does not show a distinct shift both in the calculations and experiments will be explained as follows. The situation for the $\bar{\Gamma}$ point is displayed in the bottom panel of Fig. 11. Each state of *d* band shifts with respect to the *d*-band center depending on its symmetry (bonding or antibonding). At the same time, the lattice strain changes the total energy of the system and leads to the change of the Fermi level by ΔE_F. In the present case, the shift of S3 toward the Fermi level might be nearly equal to the Fermi-level change, $\Delta S3 \sim \Delta E_F$. Photoelectron spectroscopy can measure only the relative binding energy of each state with respect to the Fermi level. Hence the S3 state is seemingly invariant in the calculated DOS and ARUPS spectra.

With the same consideration, the shift of M1 at $\bar{\mathrm{M}}$ toward the higher binding energies can be explained. The wave functions at $\bar{\mathrm{M}}$ are displayed in the middle panel of Fig. 10. The M1 peak corresponds to the state at the topmost layer which has the d_{xy} symmetry. The wave function of M1 has a large spatial distribution and merges with neighboring wave functions. This might indicate the hybridization of the d_{xy} and 4*sp* states. At the $\bar{\mathrm{M}}$ point, the d_{xy} state constructs a bonding-type Bloch function in each atomic layer (see the illustration of M1 in Fig. 11). This is consistent with the fact that M1 shifts toward the higher binding energy in the calculated DOS by the reduction of the interatomic distance.

On the other hand, according to the middle panel of Fig. 10, S4 and S5 at $\bar{\mathrm{M}}$ are attributed to the $d_{x^2-y^2}$ of the first and second layers, respectively, while B2 mainly consists of $d_{x^2-y^2}$ of the third and fourth layers. In the case of $d_{x^2-y^2}$, the wave functions make an antibonding-type Bloch function in each layer (see S4, S5, and B2 in Fig. 11). Reducing the interatomic distance laterally, the antibonding-type overlap will lead to the increase of the energy level. The apparent shifts of these states both in calculations and experiments imply that those shifts with respect to the *d*-band center are larger than the Fermi-level change. The B3 state, which did not show a shift both theoretically and experimentally, consists of $d_{3z^2-r^2}$ of several layers including the topmost layer.
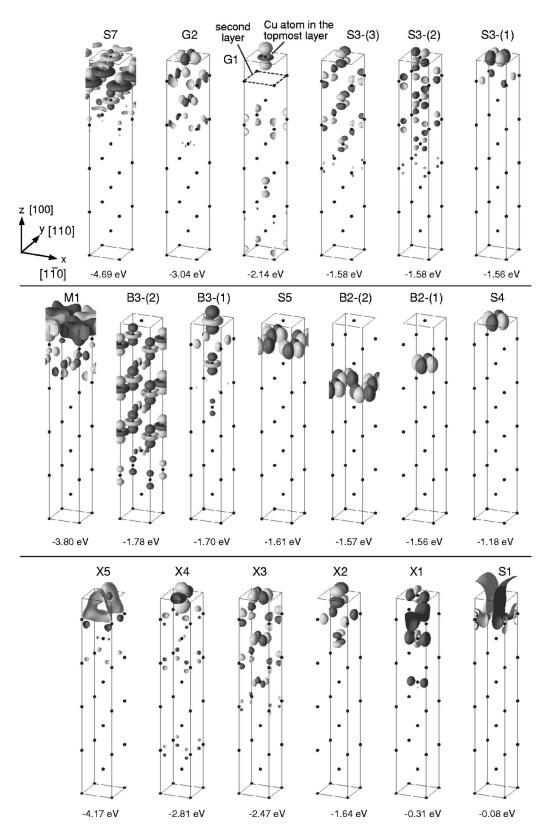
FIG. 10. The calculated wave functions of distinct energy states in the calculated DOS (Fig. 8) at $\bar{\Gamma}$ (top), at $\bar{M}$ (middle), and at $\bar{X}$ (bottom) are visualized by isosurfaces at positive (light) and negative (dark) thresholds, whose absolute values are the same value suitably taken at each k point. The small black spheres are Cu atoms. The wave functions shown here include the Bloch phase factors, $\exp(ikr)$. Several viewgraphs visualize the wave functions within extended areas from a unit cell of Cu(100). The others visualize those within a unit cell of Cu(100).
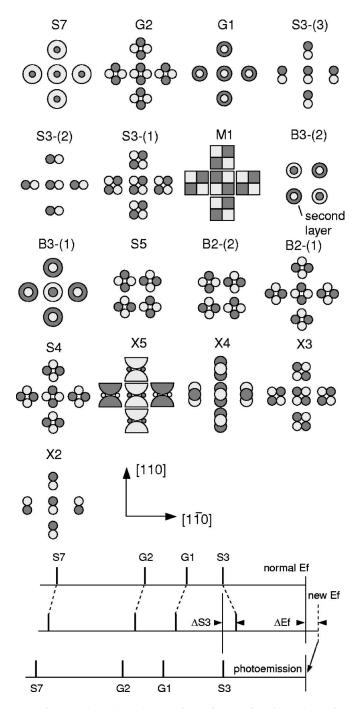
FIG. 12. The calculated work-function change versus the lattice-constant reduction ($-\%$). The work function increases with decreasing the lateral lattice constant.

Bloch function along both [110] and [1$\bar{1}$0] directions (Fig. 11). The expected shift of X2 toward the Fermi level is suppressed in the calculated DOS (bottom panel of Fig. 8) by the Fermi-level change as S3 at $\bar{\Gamma}$ and B3 at $\bar{M}$. The bonding-type Bloch functions of X4 and X5 explain well the shifts toward the higher binding energy. As for X3, this state has both bonding and antibonding characters equally. The change of Fermi level could shift this state toward the higher binding energy, though the shift is negligibly small in the calculated DOS. This indicates that the qualitative tight-binding representation is not always reliable. In particular, the tight-binding representation is not useful in explaining the behavior of extending *sp* states. According to Fig. 10, S1 and X1 mainly make bonding-type Bloch functions, while they have quite complicated spatial distributions. These states shift toward the Fermi level opposite to the rough prediction from the tight-binding representation. Thus the first-principles calculation is necessary for accurate discussion.

As a brief summary of the DOS change, the *d*-band broadening is generally observed over the SBZ, while the quantity of the broadening strongly depends on each point in the SBZ. The shift direction of each state can be understood from the symmetry of the wave function. On the other hand, it is necessary to take into account the change of the *sp* band when discussing the shift of the *d*-band center position relative to the Fermi level.

E. Work-function change induced by the lattice strain

The work function is a good index reflecting sensitively the spatial distribution of electrons at surfaces. In general, when the lateral lattice constant is reduced, the electrons spill out because the neighboring electrons tend to stay away. This leads to the increase of the surface dipole; in other words, the work function will increase. We theoretically examined the work function, which is the potential height at the center of the vacuum region in the slab model from the Fermi energy, by changing the lateral lattice constant of the Cu slab on the basis of first-principles calculations.

Figure 12 shows the calculated work functions with various lattice constants. Reducing the lateral lattice constant down to -5%, the work function ϕ increases linearly. The coefficient of the work-function change is estimated as $d\phi/da \sim -0.67$ eV/Å. Thus the theoretical results are consistent with the above intuitive expectation. When the lattice

FIG. 11. The schematic top view of wave functions shown in Fig. 10 with nearest neighbors. The symmetry of each wave function is indicated by white and/or gray colors. Only the wave functions in the topmost layer are included in the schematics except the B2, B3, and S5 at $\bar{M}$. The figures for S1 and X1 at $\bar{X}$ are not shown because of their too complicated shapes.

The shift of this state toward the Fermi level seems to be just cancelled by the Fermi-level change. We note that we picked up the most major components of B2 and B3 in Fig. 10, while these states are constructed by many other small contributions from the bulk states.

The X2, X3, X4, and X5 states consist of d_{yz}, d_{xy}, $d_{x^2-z^2}$, and broadened $d_{x^2-y^2}$ states, respectively (see the bottom panel of Fig. 10). The X2 state makes an antibonding-type
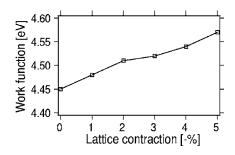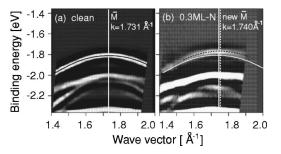
FIG. 13. Experimental band dispersion around $\bar{M}$ taken on the clean (a) and grid (b) surfaces. The solid line shows the dispersion of the Tamm state determined on the clean surface. The dotted curve indicates the dispersion observed on the grid surface.

constant was reduced by −1%, the work function is increased by 0.5%. This suggests that the chemical reactivity might be modified by the change of the sp electronic states on noble metal surfaces. This effect has not been well discussed in previous theoretical works.[4–6]

F. Estimation of the change in the lattice constant from the band dispersion

The lattice-constant reduction can be estimated from the folding point shift of the Tamm state because the Brillouin-zone enlargement reflects the reduction of the unit cell in real space. Figure 13 shows the observed band dispersion of the Tamm state on the clean surface [solid curve in Figs. 13(a) and 13(b)] and the grid surface [dotted curve in Fig. 13(b)]. Apart from the binding-energy shift of the Tamm state toward the Fermi level, we can see the shift of the folding point toward the larger wave number. A similar folding point shift was observed for the Shockley state [see Figs. 5(b) and 5(c)], while the quantitative estimation is difficult for this state.

The wave number of an electronic band is experimentally determined by the following formula explicitly including the work function:

$$k = \frac{\sqrt{2m}}{\hbar} \sqrt{h\nu - \phi + E_b} \sin \theta. \qquad (1)$$

Here m, θ, and E_b denote the electron mass, detection angle (from the surface normal), and binding energy, respectively.

On the surface with a mesoscopic pattern, such as the present case, the treatment of the work function for photoelectron spectroscopy has not been established yet; there exists a strong inhomogeneity of the work function over a few nanometers scale on this surface. There are two possible procedures for the estimation of the work function to be put in the above equation. First is to use a work function averaged over both the N-adsorbed domain and the clean Cu region. This value can be experimentally obtained from the cutoff of the secondary photoelectrons. Secondly, the local work function of the clean Cu region might be applicable to the photoelectrons from the Tamm state, which is located only in the first layer and the center of the clean region. Generally, the former treatment has been accepted because the final state of the excited photoelectron in solid is nonlocalized and ex-

tends over the nanopatterns. In the present surface, these two treatments will give lower and upper limits of the folding point shift. It is reasonable to consider that the real value lies between these two limits.

On the grid surface, the spatially averaged work function change from the clean surface was experimentally determined to be +0.286 eV by the cutoff of the secondary electrons. Then the folding point shift of the Tamm state estimated using this value is $\Delta k \sim 0.009$ Å^{-1}. This corresponds to the lattice constant reduction of $\sim -0.5\%$.

Next we try to estimate the lattice constant reduction using the local work function of the compressed clean Cu(100) surface. In this case, there are two contributions to this folding point shift: (1) lattice contraction itself and (2) increase of the work function due to the lattice contraction in terms of the first-principles calculations as discussed in the previous section. We can simply calculate the lattice-constant reduction consistently because both contributions are described as functions of the lattice constant. The shift of the wave number due to the strain-induced ϕ change at θ can be written as follows:

$$\Delta k' \sim -\frac{dk}{d\phi}\frac{d\phi}{da}\Delta a \qquad (2)$$

$$\sim \frac{\sqrt{2m}}{2\hbar} \frac{\sin \theta}{\sqrt{h\nu - \phi + E_b}} \frac{d\phi}{da}\Delta a. \qquad (3)$$

The angle θ for the He I radiation is 61°. The change of ϕ against the lattice strain was derived as $d\phi/da \sim -0.67$ eV/Å from Fig. 12. On the other hand, the relation between the folding point shift Δk^* and the lattice-constant reduction Δa around $\bar{M}$ is written as follows:

$$\Delta k^* \sim \frac{dk}{da}\Delta a = -\frac{\sqrt{2}\pi}{a^2}\Delta a. \qquad (4)$$

Then the experimentally obtained shift of the folding point Δk (~ 0.017 Å^{-1}) is approximated by the summation of these two factors,

$$\Delta k \sim \Delta k' + \Delta k^* \qquad (5)$$

$$\sim -0.039\Delta a - 0.341\Delta a \qquad (6)$$

$$\sim 0.017 \text{ Å}^{-1}. \qquad (7)$$

Thus the reduction of the lattice constant is evaluated to be $\Delta a \sim 0.045$ Å, i.e., $\sim -1.2\%$. As understood from Eq. (7), the contribution from the work-function change to the folding point shift is $\sim 10\%$ of the whole change. As a result, the real value of the lattice constant reduction is between −0.5% and −1.2%.

VII. CONCLUSION

We have studied the electronic structure change of Cu(100) due to the lattice contraction induced by partial nitrogen adsorption. Energy states at the d-band bottom (S7

state) at $\bar{\Gamma}$, *d*-band top (S4, Tamm state) at $\bar{M}$, and Shockley state (S1) were mainly investigated by means of ARUPS with synchrotron radiation (95 eV) and He I radiation (21.22 eV). We observed the shift of S7 toward the higher binding energy ($\Delta E \sim -100$ meV) at $\bar{\Gamma}$, and found the shift of the Tamm (S4) and S5 states toward the Fermi level ($\Delta E \sim +34$ meV) at $\bar{M}$. Furthermore, the shift of the Shockley state (S1) above the Fermi level was observed. The results of our first-principles calculation with a slab model agree well with these experimental results. Both the experiments and calculations indicate the broadening of the *d*-band width due to the lateral lattice-constant reduction. The symmetry of each wave function, which is calculated with the first-principles method, is consistent with the shift direction of each state by the lattice-constant reduction.

We also showed that the work function of Cu(100) is increased by the lattice-constant reduction on the basis of the first-principles calculations. This means the distinct redistribution of the Cu 4*sp* electrons in the vicinity of the surface. The lattice-constant reduction of the clean Cu surface was quantitatively estimated from the folding point shift of the

Tamm state at $\bar{M}$ by taking account of the broadening of the Brillouin zone and the change of the work function. The estimated value is between -0.5% and -1.2%.

The chemical reaction change due to the lattice strain occurs on the noble metal surfaces, in which the *d* band is filled, as well as on the transition-metal surfaces. The present results on the Cu(100) surface indicate that discussion including whole *spd* bands is necessary for the elucidation of the strain-induced chemical reaction change.

*Present address: Institute of Industrial Science, University of Tokyo, Komaba 4-6-1, Meguroku, Tokyo 153-8505, Japan. Electronic address: sekiba@iis.u-tokyo.ac.jp

†Electronic address: komori@issp.u-tokyo.ac.jp

[1] V. S. Stepanyuk, D. I. Bazhanov, A. N. Baranov, W. Hergert, P. H. Dederichs, and J. Kirschner, Phys. Rev. B **62**, 15398 (2000).

[2] O. V. Lysenko, V. S. Stepanyuk, W. Hergert, and J. Kirschner, Phys. Rev. Lett. **89**, 126102 (2002).

[3] J. Witterlin, T. Zambelli, J. Trost, J. Greeley, and M. Mavrikakis, Angew. Chem., Int. Ed. **42**, 2850 (2003).

[4] M. Mavrikakis, B. Hammer, and J. K. Nørskov, Phys. Rev. Lett. **81**, 2819 (1998).

[5] Y. Xu and M. Mavrikakis, Surf. Sci. **494**, 131 (2001).

[6] S. Sakong and A. Groβ, Surf. Sci. **525**, 107 (2003).

[7] M. Gsell, P. Jakob, and D. Menzel, Science **280**, 717 (1998).

[8] S. Ohno, K. Yagyuu, K. Nakatsuji, and F. Komori, Surf. Sci. **554**, 183 (2004).

[9] Y. Uesugi-Saitow and M. Yata, Phys. Rev. Lett. **88**, 256104 (2002).

[10] M. Yata, Y. Uesugi-Saitow, M. Kitajima, A. Kubo, and V. E. Korsukov, Phys. Rev. Lett. **91**, 206103 (2003).

[11] E. Kampshoff, E. Hahn, and K. Kern, Phys. Rev. Lett. **73**, 704 (1994).

[12] D. Sekiba, K. Nakatsuji, Y. Yoshimoto, and F. Komori, Phys. Rev. Lett. **94**, 016808 (2005).

[13] F. M. Leibsle, C. F. J. Flipse, and A. W. Robinson, Phys. Rev. B **47**, 15865 (1993).

[14] C. Cohen, H. Ellmer, J. M. Guigner, A. L'Hoir, G. Prévot, D. Schmaus, and M. Sotto, Surf. Sci. **490**, 336 (2001).

[15] S. Ohno, K. Yagyuu, K. Nakatsuji, and F. Komori, Surf. Sci. Lett. **547**, L871 (2003).

[16] C. Baldacchini, L. Chiodo, F. Allegretti, C. Mariani, M. G. Betti, P. Monachesi, and R. Del Sole, Phys. Rev. B **68**, 195109 (2003).

[17] M. Sotto, S. Gauthier, F. Pourmir, S. Rousset, and J. Klein, Surf. Sci. **371**, 36 (1997).

[18] K.-D. Lee, T. Iimori, and F. Komori, Surf. Sci. **454**, 860 (2000).

[19] S. C. Wu, C. K. C. Lok, J. Sokolov, J. Quinn, Y. S. Li, D. Tian, and F. Jona, Phys. Rev. B **39**, 13218 (1989).

[20] J. Yamauchi, M. Tsukada, S. Watanabe, and O. Sugino, Phys. Rev. B **54**, 5586 (1996).

[21] J. P. Perdew, K. Burke, and M. Ernzerhof, Phys. Rev. Lett. **77**, 3865 (1996).

[22] J. P. Perdew, K. Burke, and M. Ernzerhof, Phys. Rev. Lett. **78**, 1396 (1997).

[23] P. Heimann, J. Hermanson, H. Miosga, and H. Neddermeyer, Phys. Rev. Lett. **42**, 1782 (1979).

[24] P. Heimann, J. Hermanson, H. Miosga, and H. Neddermeyer, Phys. Rev. B **20**, 3059 (1979).

[25] S. D. Kevan, Phys. Rev. B **28**, 2268 (1983).

[26] S. D. Kevan, N. G. Stoffel, and N. V. Smith, Phys. Rev. B **31**, 3348 (1985).

[27] F. Schiller, S. V. Halilov, and C. Laubschat, Phys. Rev. B **67**, 214431 (2003).